

Magnetically polarized Ir dopant atoms in superconducting $\text{Ba}(\text{Fe}_{1-x}\text{Ir}_x)_2\text{As}_2$

M. P. M. Dean,^{1,*} M. G. Kim,^{2,†} A. Kreyssig,² J. W. Kim,³ X. Liu,¹ P. J. Ryan,³ A. Thaler,² S. L. Bud'ko,² W. Strassheim,² P. C. Canfield,² J. P. Hill,¹ and A. I. Goldman²

¹*Department of Condensed Matter Physics and Materials Science, Brookhaven National Laboratory, Upton, New York 11973, USA*

²*Ames Laboratory, US Department of Energy and Department of Physics and Astronomy, Iowa State University, Ames, Iowa 50011, USA*

³*Advanced Photon Source, Argonne National Laboratory, Argonne, Illinois 60439, USA*

(Dated: September 17, 2018)

We investigate the magnetic polarization of the Ir 5d dopant states in the pnictide superconductor $\text{Ba}(\text{Fe}_{1-x}\text{Ir}_x)_2\text{As}_2$ with $x = 0.027(2)$ using Ir L_3 edge x-ray resonant magnetic scattering (XRMS). Despite the fact that doping partially suppresses the antiferromagnetic transition, we find that magnetic order survives around the Ir dopant sites. The Ir states are magnetically polarized with commensurate stripe-like antiferromagnetic order and long correlations lengths, $\xi_{\text{mag}} > 2800$ and > 850 Å, in the ab -plane and along the c -axis, respectively, driven by their interaction with the Fe spins. This Ir magnetic order persists up to the Néel transition of the majority Fe spins at $T_N = 74(2)$ K. At 5 K we find that magnetic order co-exists microscopically with superconductivity in $\text{Ba}(\text{Fe}_{1-x}\text{Ir}_x)_2\text{As}_2$. The energy dependence of the XRMS through the Ir L_3 edge shows a non-Lorentzian lineshape, which we explain in terms of interference between Ir resonant scattering and Fe non-resonant magnetic scattering.

The discovery of superconductivity in the iron-pnictides has ignited intense interest in the interplay between magnetism and superconductivity in these compounds.^{1–4} The 122 family of pnictides, with formula $A\text{Fe}_2\text{As}_2$ where $A = \text{Ba}, \text{Ca}, \text{or Sr}$, is paramagnetic with a tetragonal crystal structure at room temperature before undergoing structural and magnetic transitions into an orthorhombic, antiferromagnetically ordered ground state.^{5–8} Various dopants can be substituted into any one of the three different atomic sites,⁹ and act to reduce the structural and magnetic transition temperatures. Doping $A\text{Fe}_2\text{As}_2$ with K,¹⁰ Co,^{11,12} Ni,^{13,14} Rh,^{15,16} P,¹⁷ Pd,^{15,16} Ir,¹⁶ Pt,¹⁸ or Ru^{19–21} induces superconductivity, although Cr,²² Mn,^{23,24} and Mo,²⁵ do not. Due to the qualitatively similar effects of many different dopants, some studies have suggested that the role of the dopants in destabilizing magnetism and inducing superconductivity is simply to act as a scattering center.^{26–28} If dopant atoms indeed act as strong scatterers, this raises the question of whether the properties of pnictides are modified around the dopant states. For example, is the local value of the magnetic order parameter suppressed to zero at the dopant sites, while remaining finite globally?

Here we exploit the Ir L_3 edge resonance to isolate the magnetic behavior of the Ir 5d dopant states in $\text{Ba}(\text{Fe}_{0.973}\text{Ir}_{0.027})_2\text{As}_2$. We demonstrate that the Ir states are magnetically polarized at low temperatures, with stripe-like commensurate magnetic order and long correlations lengths > 2800 Å in the ab -plane and > 850 Å along the c -axis. This Ir magnetic ordering disappears above T_N and is consistent with the Ir 5d states being polarized via their interaction with the Fe spins. The Ir magnetic order also co-exists microscopically with superconductivity at 5 K with no evidence for phase separation. The energy dependence of the XRMS through the Ir L_3 resonance shows a distinct non-Lorentzian lineshape

consistent with interference between resonant magnetic scattering and non-resonant magnetic scattering.

Single crystals of $\text{Ba}(\text{Fe}_{1-x}\text{Ir}_x)_2\text{As}_2$ were prepared using the self-flux solution growth method.^{12,14,15,20} Wavelength-dispersive spectroscopy was employed to measure the Ir concentration at several points on several pieces from the batch, giving an Ir concentration of $x = 0.027(2)$. Further attesting to the high sample quality, the crystalline mosaic was found to be 0.01° full width at half maximum (FWHM). The sample was shown to be superconducting with resistivity and magnetic susceptibility measurements.

XRMS experiments were performed at the 6ID-B beamline at the Advanced Photon Source (APS), following initial measurements on X22C at the National Synchrotron Light Source. The measurements at the APS were performed on a sample with a cleaved c -axis crystalline face 1×2 mm² in area with the (H, H, L) plane parallel to the vertical scattering plane. The incident x-ray beam was 1.0 mm horizontal \times 0.2 mm vertical in size and horizontally (σ) polarized. The sample was mounted on a Cu sample holder and surrounded with helium exchange gas. We checked for possible x-ray beam heating effects by comparing scans with and without attenuating the beam and we estimate that these effects are < 2 K. A graphite crystal was used as polarization analyzer before the detector to distinguish σ - σ charge scattering or fluorescence from σ - π dipole magnetic scattering, which rotates the polarization of the incident beam. At energies around the Ir L_3 edge at 11.2 keV the graphite (0, 0, 10) reflection was employed while at energies around the L_2 edge, at 12.83 keV, the (0, 0, 8) reflection was chosen.

BaFe_2As_2 crystallizes in the tetragonal ThCr_2Si_2 -type structure at room temperature with space group $I4/mmm$ (N° 139) and $a = b = 3.96$ and $c = 13.02$ Å.²⁹ Below the structural transition temperature, T_S , an or-

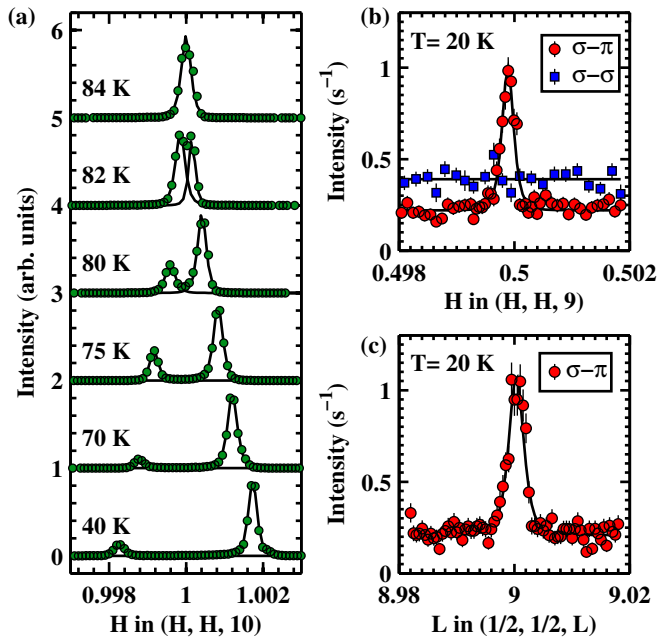


FIG. 1. (color online). (a) $(H, H, 10)_T$ scans through the $(1, 1, 10)_T$ Bragg peak at several temperatures, showing the peak splitting that occurs due to the tetragonal-orthorhombic structural transition. (b) $(H, H, 9)_T$ scans through the magnetic peak at $(\frac{1}{2}, \frac{1}{2}, 9)_T$ in $\sigma - \pi$ geometry (red \bullet) and $\sigma - \sigma$ geometry (blue \blacksquare). (c) L scan through the magnetic peak at $(\frac{1}{2}, \frac{1}{2}, 9)_T$ in $\sigma - \pi$ geometry. (b) and (c) were measured at $T = 20$ K with $E = 11.220$ keV x-rays.

thorhombic distortion sets in and the crystal assumes the $Fm\bar{3}m$ ($N^\circ 69$) space group with $a = 5.61$, $b = 5.57$ and $c = 12.95$ Å at 20 K.²⁹ In this paper we will predominantly use the tetragonal notation, and where necessary use $(H, K, L)_T$ and $(H, K, L)_O$ to distinguish tetragonal and orthorhombic notations, respectively. Figure 1(a) plots $(H, H, 10)_T$ scans through the $(1, 1, 10)_T$ Bragg peak on $\text{Ba}(\text{Fe}_{0.973}\text{Ir}_{0.027})_2\text{As}_2$. Below $T_S = 83$ K two split peaks are observed: the peak at lower H corresponds to $(2, 0, 10)_O$; while the peak at higher H corresponds to $(0, 2, 10)_O$. Below T_S we use the lower H peak to define the $(1, 1, 10)_T$ peak in the orientation-matrix. In this way $(\frac{1}{2}, \frac{1}{2}, L)_T$ corresponds to $(1, 0, L)_O$.

In order to study the Ir $5d$ dopant states, we tuned the incident x-ray energy to the Ir L_3 edge corresponding to exciting a $2p_{3/2}$ core electron into the $5d$ valence band. Figure 1(b) plots $(H, H, 9)_T$ scans through the $(\frac{1}{2}, \frac{1}{2}, 9)_T$ position at $T = 20$ K. A clear peak is present in $\sigma - \pi$ geometry and absent in $\sigma - \sigma$. This demonstrates that this peak is not associated with charge scattering such as might arise from a structural distortion. In principle $\sigma - \pi$ scattering could arise from either spin³⁰ or orbital ordering,^{31,32}. However, as we shall demonstrate, this peak has all the characteristics of magnetic order, and occurs at the same wave vector as is typically observed for magnetic order in the 122 pnictides.^{1-4,29} Thus we

conclude that it results from a magnetic polarization of the Ir $5d$ states. It should also be noted that since Ir has strong spin-orbit coupling the spin and orbital degrees of freedom are mixed. Therefore, this magnetic peak is also likely to have some partial orbital character.

The $(H, H, 9)_T$ scan in Fig. 1(b) and the L scan in Fig. 1(c) were fit with a Lorentzian-squared lineshape, shown as the black lines. The widths of the $(\frac{1}{2}, \frac{1}{2}, 9)_T$ peak along H and L are similar to that of the charge Bragg peaks, suggesting that the magnetic polarization of the Ir site is well-correlated, presumably due to coupling via the Fe spins. These widths determine lower limits on the correlation length defined as $\xi = 2a_{\text{eff}}/(2\pi w)$, where a_{eff} is the effective lattice parameter in the relevant direction and w is the peak FWHM in reciprocal lattice units (r.l.u.). We find $\xi_{\text{mag}} > 2800$ and 850 Å in the ab -plane and along the c -axis, respectively. Thus finite magnetic order survives on the Ir atom and on the neighboring Fe sites which act to polarize the Ir site. This excludes the possibility that the magnetic order parameter is locally reduced to zero around the dopant sites, as might be expected if the Ir is strongly perturbing the Fe magnetic lattice. The Ir $5d$ states may be polarized by either the local field from the Fe neighbors or via other indirect interactions between the Ir and Fe states. It is difficult to distinguish these scenarios, and in this itinerant system with extended Ir $5d$ states, both effects are likely to be at work.

It is also noteworthy that the magnetic ordering vector is commensurate with the lattice, at least to within our Q resolution of 0.0002 r.l.u. in the $[110]_T$ direction. Incommensurability in $A(\text{Fe}_{1-x}\text{M}_x)_2\text{As}_2$ was suggested on the basis of local probe measurements³³⁻³⁵ and subsequently by direct observation with neutron scattering.³⁶ For low doping $x < 0.047$, $\text{Ba}(\text{Fe}_{1-x}\text{Co}_x)_2\text{As}_2$ shows commensurate magnetic order whereas incommensurate magnetic order appears for $0.056 < x < 0.06$ before T_N is completely suppressed.³⁶ Whether the magnetic order in $\text{Ba}(\text{Fe}_{1-x}\text{Ir}_x)_2\text{As}_2$ becomes incommensurate at higher dopings will be an interesting topic for future studies.

In Fig. 2 we examine the resonant behavior of the peak. As a function of increasing incident energy, Fig. 2(a) shows the XRMS intensity at $(\frac{1}{2}, \frac{1}{2}, 9)_T$ drops slightly below the Ir absorption edge, then increases sharply through the edge, before dropping off slowly above the edge. To display the position of the absorption edge, we also plot the fluorescence yield signal obtained under the same experimental conditions. Similar resonant energy dependence of the scattered signal have been observed before at L edge XRMS, for example in heavy rare earth elements.^{37,38} For these elements the lineshape has been interpreted in terms of interference between resonant and non-resonant scattering from the same element. Here we propose that interference between Ir resonant scattering with non-resonant magnetic scattering, predominantly from the majority Fe atoms, is the cause. Although the non-resonant scattering is very weak, it has been observed in previous experiments on BaFe_2As_2 at

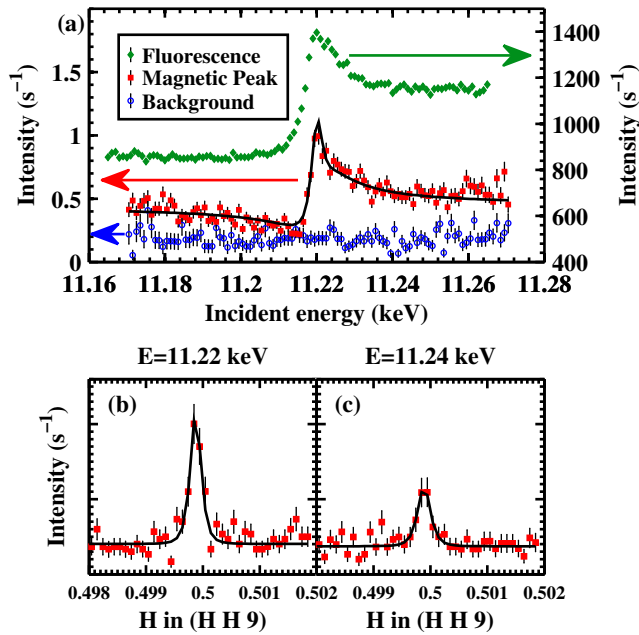


FIG. 2. (color online). The Ir resonance. (a) Energy scans through the Ir L_3 edge plotting fluorescence yield (green \diamond), magnetic peak intensity at fixed $\mathbf{Q} = (\frac{1}{2}, \frac{1}{2}, 9)_T$ (red \blacksquare) and the background scattering close to the magnetic peak (blue \bullet). All data were measured at $T = 20$ K. (b-c) $(H, H, 9)_T$ scans through the $(\frac{1}{2}, \frac{1}{2}, 9)_T$ magnetic peak with x-ray energies of (b) $E = 11.220$ keV and (c) $E = 11.240$ keV.

the same beamline,³⁹ and it is of the right order of magnitude for this explanation to hold. To test whether the proposed interference can account for this resonance, we examine the magnetic intensity $|f(E)|^2$, as a function of incident energy E , that results from the interference between a Lorentzian resonance and an energy-independent non-resonant term^{37,38}

$$|f(E)|^2 \propto \left[-\frac{\Gamma}{4} \left(\frac{m}{\hbar^2} \right) \frac{E_0^2 (F_{11} - F_{1-1})}{(E_0 - E)^2 + \Gamma^2/4} M_{\text{res}} + i \left[\frac{1}{2} \left(\frac{m}{\hbar^2} \right) \frac{E_0^2 (F_{11} - F_{1-1}) (E_0 - E)}{(E_0 - E)^2 + \Gamma^2/4} M_{\text{res}} - \frac{\hbar\omega}{mc^2} M_{\text{nonres}} \right] \right]^2. \quad (1)$$

Here E_0 is the resonant energy and Γ the FWHM of the resonance resulting from the core-hole lifetime. M_{res} and M_{nonres} are the polarization matrices for resonant and non-resonant scattering, respectively, which we approximate as constant over this energy range. Absorption effects of $< 4\%$ are neglected.³⁰ $E_0^2 (F_{11} - F_{1-1})$ is the dipole resonant scattering amplitude.

The lineshape obtained by least-squares fitting to Eq. (1) is plotted as the black line in Fig. 2(a), where a constant offset of 0.18 s^{-1} has been added to account

for the background. The resulting fit provides a good description of the data. In particular the reduction of intensity from $E = 11.170$ – 11.213 keV is difficult to explain without invoking the proposed interference.

A value of $E_0 = 11.220$ keV was obtained for the resonance energy in the XRMS, corresponding to the observed white line of the fluorescence. This is different from other insulating iridium-based compounds such as Sr_2IrO_4 ,⁴⁰ Na_2IrO_3 ,⁴¹ and $\text{Sr}_3\text{Ir}_2\text{O}_7$,⁴² where the peak in the XRMS occurs on the rising edge of the Ir L_3 fluorescence. The resonance width was also somewhat different with $\Gamma = 5.2(4)$ eV compared to values of around 8 eV in insulating iridates,⁴² these differences may reflect differences in the Ir valence or in the crystal field environment or both.

We also searched for XRMS at the Ir L_2 edge, but we were not able to find any signal, which would be consistent with the L_2 resonance intensity being too weak for us to measure.

In Fig. 3 we examine the temperature dependence of the structural and magnetic ordering in $\text{Ba}(\text{Fe}_{0.973}\text{Ir}_{0.027})_2\text{As}_2$. Figure 3(a) plots the magnitude of the orthorhombic distortion $\delta = (a - b)/(a + b)$, which becomes finite below $T_S = 82(1)$ K in a second-order phase transition. This is substantially depressed from undoped BaFe_2As_2 with $T_S = 134$ K.²⁹ On the right axis the derivative $-d\delta/dT$ is plotted to highlight a kink in δ at $74(2)$ K. X-ray scattering experiments have revealed strong magneto-elastic coupling in $\text{Ba}(\text{Fe}_{1-x}\text{Co}_x)_2\text{As}_2$, which allows us to associate the peak in $d\delta/dT$ with the Néel transition of the Fe spins at T_N .^{8,43}

Going further, the Ir L_3 edge XRMS signal plotted in Fig. 3(b), shows the magnetic polarization of the Ir $5d$ states. The ordering sets in at $70(5)$ K consistent with the T_N for which the Fe atoms order. Up to 65 K, the highest temperature at which magnetic order was observed, the Ir atoms remain well correlated with $\xi_{\text{mag}}^{\text{in-plane}} \geq 2800$ Å. The resistivity measurement in Fig. 3(c) shows changes in slope at T_S and T_N . Such changes in resistivity have been correlated with T_S and T_N previously in $\text{Ba}(\text{Fe}_{1-x}\text{Co}_x)_2\text{As}_2$.⁴⁴ The resistivity measurements also show the onset of superconductivity at 12 K. Thus in the XRMS measurements at 5 K we see Ir magnetic order coexisting with superconductivity with no measurable change in the correlation length ($\xi_{\text{mag}}^{\text{in-plane}} \geq 2800$ Å) above and below T_c . Given that the majority of Fe atoms are known to order from neutron scattering with an ordered moment of $0.60(5) \mu_B$ ⁴⁵ and the present experiment which demonstrates that magnetism can survive around the Ir atoms, this suggests a completely magnetic sample, such that superconductivity coexists microscopically with magnetism. This is consistent with local probe measurements of transition metal doped 122 pnictides,^{33,46–48} but in contrast to studies of $\text{Ba}_{1-x}\text{K}_x\text{Fe}-2\text{As}_2$.^{47,49,50}

These results establish one point in the $\text{Ba}(\text{Fe}_{1-x}\text{Ir}_x)_2\text{As}_2$ phase diagram with $x = 0.027(2)$, $T_S = 134(1)$ K, $T_N = 74(2)$ K and superconductivity be-

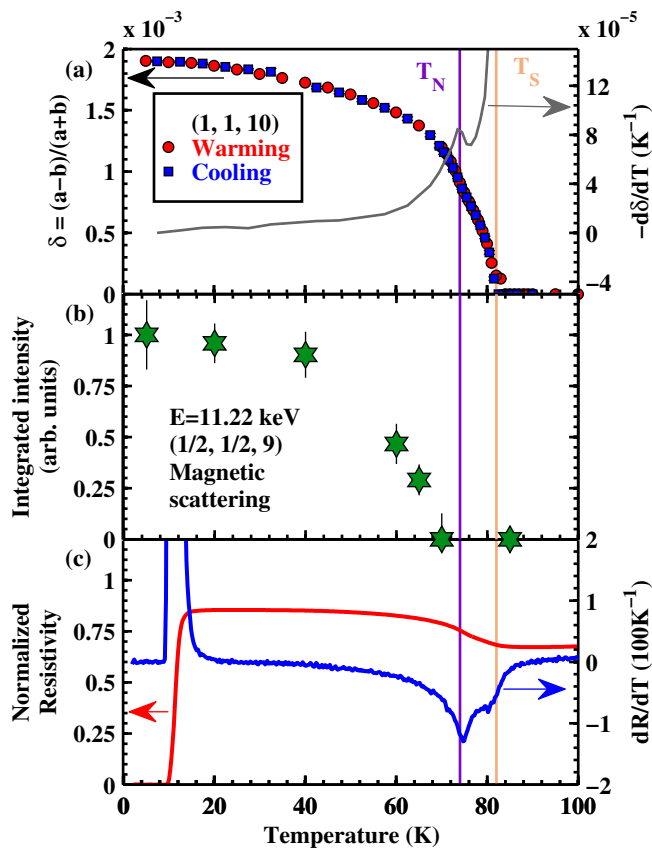


FIG. 3. (color online). The temperature dependence of the magnetic and structural order parameters. (a) The magnitude of the structural distortion $\delta = (a - b)/(a + b)$ (left axis), red \bullet denote points obtained while warming; blue \blacksquare denote points obtained while cooling. The right axis plots the derivative $d\delta/dT$ in the δ values taken while warming, which exhibits a kink that occurs at T_N . (b) The 1D integrated intensity of the magnetic peak at $(\frac{1}{2}, \frac{1}{2}, 9)_T$ measured with $E = 11.220$ keV x-rays. (c) Resistivity and the derivate of the resistivity, dR/dT showing changes in slope around T_S and T_N , and superconductivity with a 12 K onset temperature.

low 12 K. In studies of $\text{Ba}(\text{Fe}_{1-x}\text{M}_x)_2\text{As}_2$ single crystals made in the same way, T_S and T_N are reduced to zero by $x \gtrsim 0.05$ for $M=\text{Co}$ and Rh .^{9,12,14,15} Based on this single doping, Ir reduces T_S and T_N at an approximately

comparable rate. $\text{Ca}(\text{Fe}_{1-x}\text{Ir}_x)_2\text{As}_2$ also requires similar levels of doping to suppress magnetic order or to induce superconductivity.⁵¹ In measurements of powder samples of $\text{Sr}(\text{Fe}_{1-x}\text{Ir}_x)_2\text{As}_2$, Han *et al.* [Ref. 16] reported that far higher nominal doping values of $x \gtrsim 0.2$ are required to suppress magnetic or to induce superconductivity which suggests that either $\text{Sr}(\text{Fe}_{1-x}\text{Ir}_x)_2\text{As}_2$ is much less sensitive to doping than $\text{Ba}(\text{Fe}_{1-x}\text{Ir}_x)_2\text{As}_2$ or that there is a large difference between nominal and actual doping levels in $\text{Sr}(\text{Fe}_{1-x}\text{Ir}_x)_2\text{As}_2$.

To conclude, we have measured the magnetic polarization of the Ir 5d dopant states in $\text{Ba}(\text{Fe}_{0.973}\text{Ir}_{0.027})_2\text{As}_2$, which undergoes a structural phase transition at $T_S = 82(1)$ K and a Néel ordering of the majority Fe spins at $T_N = 74(2)$ K. Despite the fact that dopant atoms partially suppress T_N , we show that magnetism survives locally around the Ir sites and coexists microscopically with superconductivity at 5 K. The Ir 5d states are magnetically polarized with commensurate magnetic order and long correlation lengths $\xi_{\text{mag}} > 2800$ and 850 Å in the *ab*-plane and along the *c*-axis respectively, demonstrating that the Ir states are coupled via the Fe magnetism. This ordering sets in at 70(5) K, consistent with T_N . The XRMS intensity as a function of x-ray energy through the Ir L_3 edge shows a non-Lorentzian lineshape, which we explain in terms of interference between Ir resonant scattering and Fe non-resonant magnetic scattering.

The work at Brookhaven is supported in part under contract No. DEAC02-98CH10886 (JPH) and in part by the Center for Emergent Superconductivity (MPMD), an Energy Frontier Research Center funded by the US Department of Energy (DOE), Office of Basic Energy Sciences. Work at the Ames Laboratory was supported by the Division of Materials Sciences and Engineering, Office of Basic Energy Sciences, US DOE and is operated by Iowa State University under Contract No. DE-AC02-07CH11358. Use of the Advanced Photon Source, an Office of Science User Facility operated for the US DOE Office of Science by Argonne National Laboratory, was supported by the US DOE under Contract No. DE-AC02-06CH11357. Preliminary experiments were performed at the X22C beamline at the National Synchrotron Light Source, Brookhaven National Laboratory, which is supported by the US DOE under Contract No. DE-AC02-98CH10886.

* mdean@bnl.gov

† mgkim@iastate.edu

¹ M. D. Lumsden and A. D. Christianson, *Journal of Physics: Condensed Matter* **22**, 203203 (2010).

² D. C. Johnston, *Advances in Physics* **59**, 803 (2010).

³ P. C. Canfield and S. L. Bud'ko, *Annual Review of Condensed Matter Physics* **1**, 27 (2010).

⁴ G. R. Stewart, *Rev. Mod. Phys.* **83**, 1589 (2011).

⁵ Q. Huang, Y. Qiu, W. Bao, M. A. Green, J. W. Lynn, Y. C. Gasparovic, T. Wu, G. Wu, and X. H. Chen,

Phys. Rev. Lett. **101**, 257003 (2008).

⁶ A. I. Goldman, D. N. Argyriou, B. Ouladdiaf, T. Chatterji, A. Kreyssig, S. Nandi, N. Ni, S. L. Bud'ko, P. C. Canfield, and R. J. McQueeney, *Phys. Rev. B* **78**, 100506 (2008).

⁷ J. Zhao, W. Ratcliff, J. W. Lynn, G. F. Chen, J. L. Luo, N. L. Wang, J. Hu, and P. Dai, *Phys. Rev. B* **78**, 140504 (2008).

⁸ M. G. Kim, R. M. Fernandes, A. Kreyssig, J. W. Kim, A. Thaler, S. L. Bud'ko, P. C. Canfield, R. J. McQueeney, J. Schmalian, and A. I. Goldman,

- Phys. Rev. B **83**, 134522 (2011).
- ⁹ N. Ni and S. L. Bud'ko, MRS Bulletin **36**, 620 (2011).
 - ¹⁰ M. Rotter, M. Tegel, and D. Johrendt, Phys. Rev. Lett. **101**, 107006 (2008).
 - ¹¹ A. S. Sefat, R. Jin, M. A. McGuire, B. C. Sales, D. J. Singh, and D. Mandrus, Phys. Rev. Lett. **101**, 117004 (2008).
 - ¹² N. Ni, M. E. Tillman, J.-Q. Yan, A. Kracher, S. T. Hannahs, S. L. Bud'ko, and P. C. Canfield, Phys. Rev. B **78**, 214515 (2008).
 - ¹³ L. J. Li, Y. K. Luo, Q. B. Wang, H. Chen, Z. Ren, Q. Tao, Y. K. Li, X. Lin, M. He, Z. W. Zhu, G. H. Cao, and Z. A. Xu, New Journal of Physics **11**, 025008 (2009).
 - ¹⁴ P. C. Canfield, S. L. Bud'ko, N. Ni, J. Q. Yan, and A. Kracher, Phys. Rev. B **80**, 060501 (2009).
 - ¹⁵ N. Ni, A. Thaler, A. Kracher, J. Q. Yan, S. L. Bud'ko, and P. C. Canfield, Phys. Rev. B **80**, 024511 (2009).
 - ¹⁶ F. Han, X. Zhu, P. Cheng, G. Mu, Y. Jia, L. Fang, Y. Wang, H. Luo, B. Zeng, B. Shen, L. Shan, C. Ren, and H.-H. Wen, Phys. Rev. B **80**, 024506 (2009).
 - ¹⁷ S. Kasahara, T. Shibauchi, K. Hashimoto, K. Ikeda, S. Tonegawa, R. Okazaki, H. Shishido, H. Ikeda, H. Takeya, K. Hirata, T. Terashima, and Y. Matsuda, Phys. Rev. B **81**, 184519 (2010).
 - ¹⁸ S. R. Saha, T. Drye, K. Kirshenbaum, N. P. Butch, P. Y. Zavalij, and J. Paglione, Journal of Physics: Condensed Matter **22**, 072204 (2010).
 - ¹⁹ S. Sharma, A. Bharathi, S. Chandra, V. R. Reddy, S. Paulraj, A. T. Satya, V. S. Sastry, A. Gupta, and C. S. Sundar, Phys. Rev. B **81**, 174512 (2010).
 - ²⁰ A. Thaler, N. Ni, A. Kracher, J. Q. Yan, S. L. Bud'ko, and P. C. Canfield, Phys. Rev. B **82**, 014534 (2010).
 - ²¹ M. G. Kim, D. K. Pratt, G. E. Rustan, W. Tian, J. L. Zarestky, A. Thaler, S. L. Bud'ko, P. C. Canfield, R. J. McQueeney, A. Kreyssig, and A. I. Goldman, Phys. Rev. B **83**, 054514 (2011).
 - ²² K. Marty, A. D. Christianson, C. H. Wang, M. Matsuda, H. Cao, L. H. VanBebber, J. L. Zarestky, D. J. Singh, A. S. Sefat, and M. D. Lumsden, Phys. Rev. B **83**, 060509 (2011).
 - ²³ Y. Liu, D. Sun, J. Park, and C. Lin, Physica C **470**, S513 (2010).
 - ²⁴ A. Thaler, H. Hodovanets, M. S. Torikachvili, S. Ran, A. Kracher, W. Straszheim, J. Q. Yan, E. Mun, and P. C. Canfield, Phys. Rev. B **84**, 144528 (2011).
 - ²⁵ A. S. Sefat, K. Marty, A. D. Christianson, B. Saparov, M. A. McGuire, M. D. Lumsden, W. Tian, and B. C. Sales, Phys. Rev. B **85**, 024503 (2012).
 - ²⁶ H. Wadati, I. Elfimov, and G. A. Sawatzky, Phys. Rev. Lett. **105**, 157004 (2010).
 - ²⁷ M. G. Vavilov and A. V. Chubukov, Phys. Rev. B **84**, 214521 (2011).
 - ²⁸ R. S. Dhaka, C. Liu, R. M. Fernandes, R. Jiang, C. P. Strehlow, T. Kondo, A. Thaler, J. Schmalian, S. L. Bud'ko, P. C. Canfield, and A. Kaminski, Phys. Rev. Lett. **107**, 267002 (2011).
 - ²⁹ M. Rotter, M. Tegel, D. Johrendt, I. Schellenberg, W. Hermes, and R. Pöttgen, Phys. Rev. B **78**, 020503 (2008).
 - ³⁰ J. P. Hill and D. F. McMorrow, Acta Crystallographica Section A **52**, 236 (1996).
 - ³¹ S. B. Wilkins, P. D. Spencer, P. D. Hatton, S. P. Collins, M. D. Roper, D. Prabhakaran, and A. T. Boothroyd, Phys. Rev. Lett. **91**, 167205 (2003).
 - ³² U. Staub, V. Scagnoli, A. M. Mulders, K. Katsumata, Z. Honda, H. Grimmer, M. Horisberger, and J. M. Tonnerre, Phys. Rev. B **71**, 214421 (2005).
 - ³³ Y. Laplace, J. Bobroff, F. Rullier-Albenque, D. Colson, and A. Forget, Phys. Rev. B **80**, 140501 (2009).
 - ³⁴ P. Bonville, F. Rullier-Albenque, D. Colson, and A. Forget, EPL (Europhysics Letters) **89**, 67008 (2010).
 - ³⁵ A. Błachowski, K. Ruebenbauer, J. Żukrowski, K. Rogacki, Z. Bukowski, and J. Karpinski, Phys. Rev. B **83**, 134410 (2011).
 - ³⁶ D. K. Pratt, M. G. Kim, A. Kreyssig, Y. B. Lee, G. S. Tucker, A. Thaler, W. Tian, J. L. Zarestky, S. L. Bud'ko, P. C. Canfield, B. N. Harmon, A. I. Goldman, and R. J. McQueeney, Phys. Rev. Lett. **106**, 257001 (2011).
 - ³⁷ J. W. Kim, Y. Lee, D. Wermeille, B. Sieve, L. Tan, S. L. Bud'ko, S. Law, P. C. Canfield, B. N. Harmon, and A. I. Goldman, Phys. Rev. B **72**, 064403 (2005).
 - ³⁸ D. Gibbs, G. Grübel, D. R. Harshman, E. D. Isaacs, D. B. McWhan, D. Mills, and C. Vettier, Phys. Rev. B **43**, 5663 (1991).
 - ³⁹ M. G. Kim, A. Kreyssig, Y. B. Lee, J. W. Kim, D. K. Pratt, A. Thaler, S. L. Bud'ko, P. C. Canfield, B. N. Harmon, R. J. McQueeney, and A. I. Goldman, Phys. Rev. B **82**, 180412 (2010).
 - ⁴⁰ B. J. Kim, H. Ohsumi, T. Komesu, S. Sakai, T. Morita, H. Takagi, and T. Arima, **323**, 1329 (2009).
 - ⁴¹ X. Liu, T. Berlijn, W.-G. Yin, W. Ku, A. Tsvelik, Y.-J. Kim, H. Gretarsson, Y. Singh, P. Gegenwart, and J. P. Hill, Phys. Rev. B **83**, 220403 (2011).
 - ⁴² S. Boseggia, R. Springell, H. C. Walker, A. T. Boothroyd, D. Prabhakaran, D. Wermeille, L. Bouchenoire, S. P. Collins, and D. F. McMorrow, ArXiv e-prints arXiv:1201.1452.
 - ⁴³ S. Nandi, M. G. Kim, A. Kreyssig, R. M. Fernandes, D. K. Pratt, A. Thaler, N. Ni, S. L. Bud'ko, P. C. Canfield, J. Schmalian, R. J. McQueeney, and A. I. Goldman, Phys. Rev. Lett. **104**, 057006 (2010).
 - ⁴⁴ D. K. Pratt, W. Tian, A. Kreyssig, J. L. Zarestky, S. Nandi, N. Ni, S. L. Bud'ko, P. C. Canfield, A. I. Goldman, and R. J. McQueeney, Phys. Rev. Lett. **103**, 087001 (2009).
 - ⁴⁵ M.G. Kim *et al.* unpublished.
 - ⁴⁶ M.-H. Julien, H. Mayaffre, M. Horvatic, C. Berthier, X. D. Zhang, W. Wu, G. F. Chen, N. L. Wang, and J. L. Luo, Europhysics Lett. **87**, 37001 (2009).
 - ⁴⁷ J. T. Park, D. S. Inosov, C. Niedermayer, G. L. Sun, D. Haug, N. B. Christensen, R. Dinnebier, A. V. Boris, A. J. Drew, L. Schulz, T. Shapoval, U. Wolff, V. Neu, X. Yang, C. T. Lin, B. Keimer, and V. Hinkov, Phys. Rev. Lett. **102**, 117006 (2009).
 - ⁴⁸ P. Wang, Z. M. Stadnik, J. Żukrowski, A. Thaler, S. L. Bud'ko, and P. C. Canfield, Phys. Rev. B **84**, 024509 (2011).
 - ⁴⁹ H. Fukazawa, T. Yamazaki, K. Kondo, Y. Kohori, N. Takeshita, P. M. Shirage, K. Kihou, K. Miyazawa, H. Kito, H. Eisaki, and A. Iyo, Journal of the Physical Society of Japan **78**, 033704 (2009).
 - ⁵⁰ T. Goko, A. A. Aczel, E. Baggio-Saitovitch, S. L. Bud'ko, P. C. Canfield, J. P. Carlo, G. F. Chen, P. Dai, A. C. Hamann, W. Z. Hu, H. Kageyama, G. M. Luke, J. L. Luo, B. Nachumi, N. Ni, D. Reznik, D. R. Sanchez-Candela, A. T. Savici, K. J. Sikes, N. L. Wang, C. R. Wiebe, T. J. Williams, T. Yamamoto, W. Yu, and Y. J. Uemura, Phys. Rev. B **80**, 024508 (2009).
 - ⁵¹ Y. Qi, Z. Gao, L. Wang, X. Zhang, D. Wang,

C. Yao, C. Wang, C. Wang, and Y. Ma,
Europhysics Lett. **96**, 47005 (2011).